Analysis on experimental valence charge density in germanium at RT and 200 K

ARTICLE *in* JOURNAL OF PHYSICS AND CHEMISTRY OF SOLIDS · AUGUST 2009

Impact Factor: 1.85 · DOI: 10.1016/j.jpcs.2009.07.002

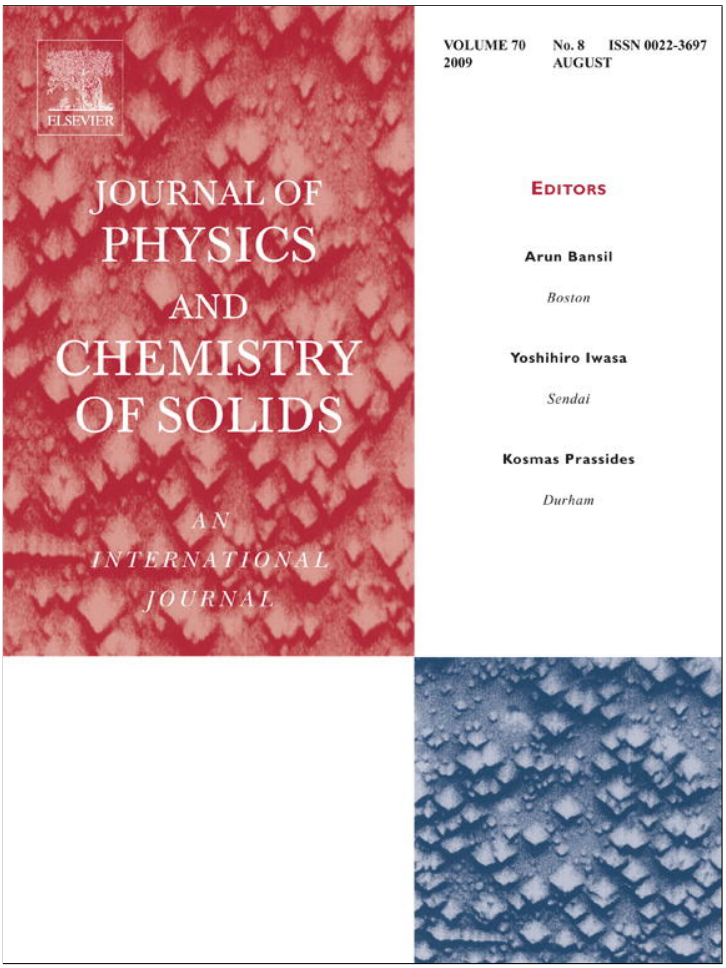

Journal of Physics and Chemistry of Solids 70 (2009) 1185–1194

Contents lists available at ScienceDirect

Journal of Physics and Chemistry of Solids

journal homepage: www.elsevier.com/locate/jpcs

Analysis on experimental valence charge density in germanium at RT and 200 K

S. Israel [a,*], K.S. Syed Ali [b], R.A.J.R. Sheeba [b], R. Saravanan [c]

[a] Department of Physics, The American College, Madurai 625 002, India
[b] Department of Physics, Yadava College, Madurai 625 014, India
[c] Department of Physics, The Madura College, Madurai 625 011, India

ARTICLE INFO

Article history:
Received 19 December 2008
Received in revised form
15 May 2009
Accepted 1 July 2009

Keywords:
A. Semiconductor
C. X-ray diffraction
D. Electronic structure

ABSTRACT

The electronic structure and hence the valence charge distribution of germanium at 296 and 200 K has been elucidated from structure factors measured by X-ray diffraction experiment using maximum entropy method (MEM) and multipole model. The methods adopted here are used to extract the fine details of the charge density distribution in the valence region. The charge density evaluated using both the models along the bond path and at the mid bond positions are compared and found to confirm the covalent bond existing in the solid. Topology of the charge density in the crystal is analysed and the critical points determined reveal unique spatial arrangement of valence charge in the direction normal to the bonding direction. The Laplacian of the charge density is also analysed for the understanding of the spatial distribution and the partitioning of the valence charge. The local charge concentration and the mapping of the electron pairs of the Lewis and valence shell electron pair repulsion (VSEPR) models have been done using electron localization function (ELF) and localized orbital locator (LOL).

1. Introduction

The role of elemental semiconductors like silicon and germanium in electronics industry is commended by their enormous usage. The quantum free electron theory gives us the importance of free electrons and their role in deciding some of the electrical characteristics and parameters. Hence, the study on the arrangement of charges and their distribution in space becomes more important and it turns out to be meaningful by experimental crystallographic methods. The qualitative and quantitative analyses of the valence region in these compounds become more important in order to understand their electronic characteristics.

The information of inside picture from the unit cell of single crystals by X-ray diffraction is the authentic tool used for analyzing charge density. The determination of charge density using conventional Fourier analysis of observed X-ray structure factors has its own limit due to the unrealistic negative charge densities and so a perfect understanding of the charge distribution in solids needs to have a fool proof method. One such method deals on statistically analyzing the experimentally observed structure factors by enforcing the entropy in the charge density calculated from them. The method, maximum entropy method (MEM), has enormous respect from the crystallographers due to its reproducibility of the true charge density distribution in a unit cell but is seldom used by amateurs, as it requires the best computing ability and vector computers. The authors have tried this method for various simple, high symmetric systems and the results have produced some of the most interesting results [1,2]. The understanding of bonding from the density profiles and the estimation of ionicity, charge transfer in the materials and the accuracy in reproducing the charge density pictures without unrealistic negative points have given high credits to the method adopted in this study.

The understanding of the valence charge and the contribution of various orbitals to it can be qualitatively and quantitatively elucidated using the multipole model as proposed by Hansen and Coppens [3]. The charge density (ρ) and other parameters like $\nabla\rho(r)$ and $\nabla^2\rho(r)$ can be used as tools to identify and analyze valence shell charge concentration (VSCC). The analysis of the valence region, particularly on the localization of orbitals and the like-spin electrons can be done using localized orbital locator (LOL) [4] and the electron localization function (ELF) [5]. This information is critical in understanding the electronic behavior of the semiconductors. In this work Ge has been studied for the visual of charge density in the valence density region and also the spatial distribution of localized charges and orbitals using charge density in the unit cell derived using MEM and Multipole models.

2. Experiment

A bulk crystal of germanium (Purity 99.99%) was cut into pieces and spherized using Nonius spherizer and etched with

* Corresponding author. Tel.: +91 9865384403.
E-mail address: israel.samuel@gmail.com (S. Israel).

0022-3697/$ - see front matter © 2009 Elsevier Ltd. All rights reserved.
doi:10.1016/j.jpcs.2009.07.002

suitable etching solutions to remove the strained surfaces. A good quality crystal with radius 0.19(1) mm was chosen from them (see Fig. 1) and the X-ray diffraction data sets at temperatures 296 and 200 K were collected using CAD-4 X-ray diffractometer with MoKα as the radiation and graphite as the monochromator. The data sets were collected for a full sphere up to $2\theta = 90^\circ$ with several psi-scan sets resulting in the transmission factor of about 1. Three standard reflections were monitored for every 2 h ($0.99 < \text{decay} < 1.0056$) and 25 reflections were used for the cell refinements. The full data set was collected in the θ range of 1.5°–45° at 296 and 200 K for the present study. Liquid nitrogen stream was used for achieving low temperatures while similar experimental conditions were maintained for all the data collected at these temperatures.

3. Least squares refinement

Germanium has a diamond structure with $Fd\bar{3}m$ space group. Cell refinement was done with the intensity data collected in the θ range of 6.00°–16.96° at RT and from 10.258° to 15.899° at 200 K, respectively. The refined cell parameter and the volume of the unit cell are given in the Table 1. The cell parameter measured at room temperature is in close agreement with the literature value (i.e., $a_0 = 6.6579$ Å at 298 K [6]). The standard full matrix least squares method is used for correcting the raw data for absorption, extinction and TDS effects. Both the data sets were refined using harmonic model while incorporating the absorption [7] and extinction effects using Zachariasen model [8]. Other parameters and the reliability indices are given in Table 1. The thermal parameters (B) thus refined show the expected decreasing trend with respect to the decreasing temperature.

Fig. 1. Sphere of Ge chosen for the experiment.

Table 1
Parameters from the least squares refinement.

Parameters	RT	200 K
a_o (Å)	5.6416(6)	5.6395(6)
Volume (Å^3)	179.56(3)	179.36(3)
B (Å^2)	0.452(17)	0.360(35)
R (%)	1.74	2.53

4. Charge density analysis in the unit cell

For the reconstruction of electron density distribution we have used the modified electron density model proposed by Hansen and Coppens [3] with the option that allows the refinement of population parameters at various orbital levels where the atomic density is described as a series expansion in real spherical harmonic functions through fourth order Y_{lm}. According to this model, the charge density in a crystal is written as the superposition of harmonically vibrating aspherical atomic density distribution convolving with the Gaussian thermal displacement distribution as $\rho(\vec{r}) = \sum_k^{atoms} \rho_k(\vec{r} - \vec{r}_k - \vec{u}) \otimes t_k(\vec{u})$, where $t_k(\vec{u})$ is the Gaussian term and the symbol $\otimes$ indicates a convolution. The atomic charge density is then defined as

$$\rho(\vec{r}) = P_c\rho_{core}(\vec{r}) + P_v\kappa'^3\rho_{valence}(k'r) + \sum_{l=0}^{4}\kappa''^3 R_l(\kappa'' r)\sum_{m=-l}^{l} P_{lm}Y_{lm}(\vec{r}/r)$$

where P_c, P_v and P_{lm} are population coefficients. Canonical Hatree–Fock atomic orbitals of the free atoms normalized to one electron were used for the construction of ρ_{core} and $\rho_{valence}$, but the valence function is allowed to expand and contract by the adjustment of the variable parameters κ' and κ''.

After successful refinement on the structural parameters the structure factors were used for the core and the valence and the pseudo-atomic electron occupancies P_{lm} using the software JANA 2006 [9]. The neutral atom wave functions are taken from Clementi tables [10] and the Slater type radial functions are used with $n_l = 4,4,6,8$ for $l \leq 4$ according to Hansen and Coppens [3]. The atomic orbitals up to hexadecapole were considered with double zeta function ξ taken as per Lu et al. [11] and has a value 1.913 a.u^{-1}. As described by Dawson [12] and Stewart [13] the multipole deformation functions allowed for the tetrahedral site symmetry of the germanium atom are one octapole (i.e. P_{32-}) and one hexadecapole, the latter being a combination of P_{40} and P_{44} while the other terms vanish due to the symmetry of the Ge atom being $m\bar{3}m$. A physically more acceptable argument is that the higher functions effectively account for density in the covalent bond region, which are relatively distant from the nuclear centers. During the refinement, the core is taken as Ar atom and the valence expansion/contraction parameter (κ'') is refined for both the data sets measured at RT and 200 K. The unit cell electron neutrality condition was imposed during the multipole refinement. The parameters refined show good agreement with the already available literature values and are presented as Table 2. The refined κ'' parameter shows the expansion of the valence region for both the data sets as agreed upon by Lu et al. [11]. The reliability indices and the Goodness of Fit factors (GoF) confirm the accuracy with which the results are produced and can be credited accordingly.

Topology of the electron density provides a faithful mapping of the concept of atoms, bonds and structure and hence charge distribution constructed using Multipole model is analysed using "Atoms in molecules (AIM) theory" as proposed by Bader [14]. According to him "two atoms are bonded if they are connected by a line of maximum electron density called bond path, on which lies a bond critical point (BCP) where $\vec{\nabla}\rho(r_{BCP}) = 0$, and the critical points are the characteristics of the bonding existing between the atoms". The critical points are searched in the charge density distribution at RT and 200 K using Newton–Raphson method and

Table 2
Parameters from multipole refinement.

Parameters	Ge at RT	Ge at 200 K	Ge at RT[a]	Ge at RT[b]
P_c	Ar (18.0)	Ar (18.0)	Ar (18.0)	Ar (18.0)
$P\nu$	14.305	14.637	–	–
κ'	0.986	0.973	0.955	0.922
κ''	1.033	1.041	–	–
P_{32-}	0.552	0.011	0.583	0.353
P_{40}	−0.558	−0.359	−0.510	−0.333
P_{44+}	−0.413	−0.266	–	−0.247
P_{44+}	0.7404*P_{40}	0.7404*P_{40}	–	0.74045*P_{40}
B (Å^2)	0.501	0.387	–	–
R (%)	1.71	2.54	0.189	1.60
GoF	0.91	1.29	1.98	1.07

[a] Lu et.al. [11].
[b] Avilov et al. [15].

Table 3
Critical points from topological analysis.

Temp.	Type	x	y	z	λ_1	λ_2	λ_3	ρ	$\nabla^2\rho$
RT	(3,−3)	0.00	0.00	0.00					
	(3,−1)	−0.125	0.125	−0.125	−0.63	−0.63	3.39	0.30	−2.14
	(3,+1)	0.00	0.00	0.3375	−0.21	0.19	0.5	0.08	0.48
	(3.+3)	0.00	0.00	0.50	0.01	0.01	0.01	0.08	0.02
	(3.+3)	0.125	0.125	0.625	0.13	0.13	0.19	0.04	0.46
200 K	(3,−3)	0.00	0.00	0.00					
	(3,−1)	−0.125	0.125	−0.125	−0.67	−0.67	2.83	0.35	−1.49
	(3,+1)	0.00	0.00	0.3375	−0.16	0.17	0.17	0.08	0.18
	(3.+3)	0.00	0.00	0.50	0.13	0.13	0.13	0.04	0.38
RT[a]	(3,−1)	−0.125	0.125	−0.125	−1.87	−1.87	2.04	0.575	−1.70
	(3,+1)	0.00	0.00	0.3375	−0.02	0.013	0.013	0.027	0.24
	(3.+3)	0.00	0.00	0.50	0.05	0.05	0.05	0.024	0.15
RT[b]	(3,−1)	−0.125	0.125	−0.125	−1.43	−1.43	1.68	0.504	−1.18
	(3,+1)	0.00	0.00	0.3375	−0.02	0.014	0.014	0.03	0.26
	(3.+3)	0.00	0.00	0.50	0.02	0.05	0.05	0.022	0.15
RT[c]	(3,−1)	−0.125	0.125	−0.125	−0.65	−0.65	1.85	0.357	0.55

[a] Avilov et al. [15].
[b] Abramov et al. [17].
[c] From the characteristics of the pro-crystal of germanium [16].

are given in Table 3. From the values of $\rho(r_{BCP})$ we can conclude that the estimation of the parameters for both the data sets is accurate enough to be compared with the electron diffraction data [15]. According to Tsierelson [16] closed shell interactions will have low $\rho(r_{BCP})$ i.e., $0.07<\rho(r_{BCP})<0.25\,e/Å^3$ and $0.12<|\lambda_1|/\lambda_3<0.17$ and for shared shell interactions $\rho(r_{BCP})$ will be high i.e., $0.30<\rho(r_{BCP})<2.0\,e/Å^3$, $|\lambda_1|/\lambda_3>0.17$ and $\nabla^2\rho(r_{BCP})<0$. The requirements met by both the data sets confirm the fact that the derived charge density distribution enacts the expected covalent behavior.

For the charge integration, a basin around the atom is established by identifying a surface called zero-flux surface (ZFS) or inter-atomic surface (IAS), which is a topological manifold that separates atoms and consists of bundle of gradient paths terminating at BCP between two atoms, characterized by the condition $\hat{n}\cdot\vec{\nabla}\rho(\vec{r})=0$ for all points on a surface and $\forall\vec{r}\in S$. The basin integration done with minimal ZFS distance (coinciding with r_{BCP}, i.e., 1.221 Å), results in the atomic charge of 3.07 e^-, for both the data sets amounts to the shared charge of 0.7675 e^- per bond per atom in the bonding directions. This value is less compared to the conventional understanding of 1 e^- contribution each per bond due to the fact that the bonding charge may have spread across the non-bonding direction thus making the atoms look more aspherical when bonded.

The want of more clear visualization of the valence region and the understanding of bonding charge spreading over the space along the bond path has motivated the authors to try another method of reconstructing the charge density using maximum entropy method, which is unbiased to any theoretical model and produces no unphysical negative charge density but the high resolution true charge density with clear bonding features.

5. Valence charge density analysis

The method used to obtain the valence charge density along the bond path is the one proposed by Collins [18] based on the statistical approach, maximum entropy method. According to him, the entropy in evaluating the charge density in an iterative cycle at the ith pixel in a unit cell is maximized in terms of the assumed uniform prior density at that pixel until a weak constraint C as proposed by Sakata and Sato [19], defined as below, that compares the observed and calculated structure factors, becomes 1

$$C=\frac{1}{N}\sum_k\frac{|F_{CAL}(k)-F_{OBS}(k)|^2}{\sigma^2(k)}.$$

The resulting charge density is the required ρ_{MEM} and is given as

$$\rho_{\mathrm{MEM}}(\mathbf{r}_i)=\tau(\mathbf{r}_i)\exp\left\{\frac{\lambda F_{000}}{N}\left[\sum\frac{1}{\sigma(k)^2}\right]\times|\mathrm{F_{obs}}\cdot(\mathbf{k})-\mathrm{F_{cal}}\cdot(\mathbf{k})|\exp(-2\pi\mathrm{j}\cdot\mathbf{k}\cdot\mathbf{r})\right\}$$

Here F_{000} is the number of electrons in the unit cell and $\tau(\mathbf{r}_i)$ is the prior density assigned to the ith pixel. And N, F_{Obs} ($\mathbf{k}$), F_{Cal} ($\mathbf{k}$) and $\sigma(\mathbf{k})$ are the number of available reflections, observed and calculated structure factors and standard deviations of the observations, respectively.

The structure factors refined for structural parameters were used for the MEM procedure to obtain the charge density distribution in a unit cell along with a weak constraint. Initially, the unit cell is divided into $64\times64\times64$ pixels and each pixel is uniformly filled with prior density whose value is F_{000}/a_0^3. The structure factors were calculated iteratively while increasing the entropy in charge density in every cycle until the convergence criterion C becomes 1 under minimum possible iterations. In our case, it took 710 and 430 iterations for the data set measured at RT and 200 K. The requirement of accurate structure factors for the study on charge density is verified by histograms plotted with weighted differences between the observed and the MEM structure factors versus the number of reflections (Fig. 2). The histograms for both the data sets show that most of the reflections have least possible error. Also, the error map (Fig. 3) in the reciprocal lattice space in which the reflections were measured confirms the fact that even the reflections measured at lower angles have least possible errors, which is a very good trend for the calculation of charge density in the chosen system. The residuals given in Table 4 show the accuracy of the data and the results can be credited accordingly. The resultant charge density distribution with the resolution given in Table 4 can give accurate reliable information about the bonding especially in the valence region that is the prime interest of the study.

The charge density thus evolved inside the unit cell is plotted using the visualization software VESTA [20] and is presented here as Fig. 4(a) and (b). These figures plotted at the isosurface level 0.46 for RT and 0.32 for 200 K show the unique charge density of

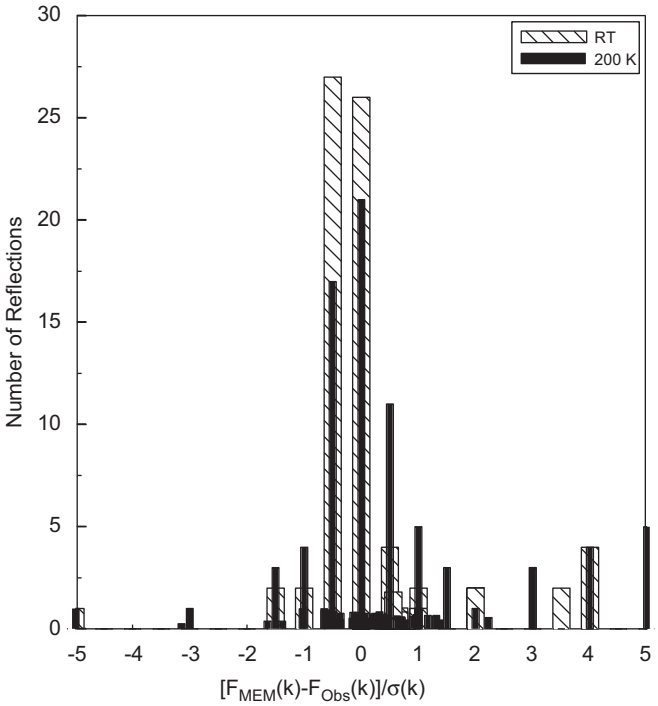

Fig. 2. Histogram of observed number of reflections.

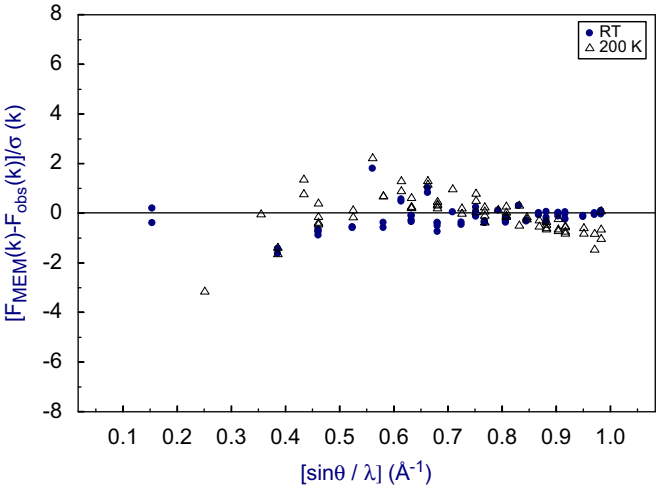

Fig. 3. Error distributions of the observations in the reciprocal space.

Table 4
Parameters from the MEM analyses.

Parameters	RT	200 K
Number of reflections, N	69	69
Prior density, $\tau(r_i)$ (e/Å^3)	1.4257	1.4273
Lagrange parameter, λ	0.1	0.1
Number of Iterations	710	430
R (%)	1.24	1.80
wR (%)	1.81	2.32
Resolution (Å/pixel)	0.08815	0.08812

the valence region arranged in the direction perpendicular to the bond path. The valence charge density forms a solid ring like structure with a maximum in the middle and also at the center of the solid ring. The reduction in the atomic charge while the charge integration is done on the atomic basin is actually due to the exclusion of this charge while identifying ZFS. Wang and Klein [21] have observed this phenomenon in their determination of self-consistent electronic structure of germanium using Gaussian orbitals method with local density form of the exchange correlation functional. Lu et al. [6] have also observed this while deriving charge density distribution from high accurate structure factors measured using γ-ray measurements and multipole expansion model of the charge densities. To understand this and to analyze, the charge density distribution map upon $(1\,\bar{1}\,0)$ plane is plotted in the density range of 0.35–3.0 e/Å^3 with the contour interval of 0.1325 e/Å^3 (Fig. 5(a) and (b)). These figures show the Ge atoms at the corners and show no unrealistic negative density, which is the characteristic of the MEM procedure. The spherical nature of the atoms and the accumulation of the charges towards the charge center as we reduce the temperature can also be visualized from these maps. The same phenomenon thus explains the decrease in the Debye–Waller factor under lowered temperature environment.

A clear visualization of this valence charge is made possible in Fig. 6(a) and (b) plotted in the range of 0.35–2.05 e/Å^3 with the contour interval 0.085 e/Å^3. These figures clearly indicate that the bonding charges in Ge actually exist perpendicular to the bonding direction and the reason could be the space in which the bond charge is spread over. We were curious in finding the size of the bonding charge and their spread in the space available. In doing so we have plotted the one-dimensional charge density profile along [111] direction (Fig. 7) for both the data sets and is compared with the charge density constructed using structure factors derived using local density approximation formalism (LDA) [21] and also from the compiled structure factors by Lu et al. [11].

Fig. 7 shows the core of the corner atom ends at 0.916 Å and the region of bond charge begin from there and extends up to 1.526 Å where the nearest neighbor begins its territory. This gives the magnitude of the extent of the bonding charge (i.e., 0.6105 Å) along the bonding direction for both the data sets. We have estimated the spread of the bond charge for both the data sets and found them as 1.2677 Å (diameter of the outer ring) and 1.3452 Å measured at RT and 200 K, respectively. This indicates that the bonding charges can no way exist along the bonding direction and so the system has to accommodate them only in the free space, which is in the direction perpendicular to the bonding direction. Also a small build up of charges is observed and this non-nuclear maxima (NNM) is placed exactly at the mid bond position. This position (see Table 5) is the same for both the data sets, which coincides with the tetrahedral covalent radius (sp^3 hybrids) of the atom (i.e., r_c(Ge) = 1.22 Å [22]). This confirms the fact that the charge accumulated at the mid bond is because of the quantum mechanical effect of sharing electrons, for the bonding, from the valence orbitals and thus the bonding is confirmed to be covalent. The density measured at this position is having a magnitude of 0.555 and 0.525 e/Å^3 for the data measured at 296 and 200 K, respectively. This density estimated by Lu et al. [6] is in the range of 0.46 and 0.58 e/Å^3 and thus our estimation coincides very well with Lu et al. [6]. The magnitude of the NNM can be compared with 0.67 e/Å^3 for GaP, 0.568 e/Å^3 for Si and 1.49 e/Å^3 for diamond, [23] etc. The same behavior is seen in Ge confirms that the system is as covalent as silicon. The LDA method, however, could not reproduce the covalent behavior of the solid and hence the charge density along [111] do not seem to have a NNM at the mid bond position. The same is true for the charge density due to Lu et al. [11]. But the behavior of charge density along the bonding region is reproduced and it becomes a very good tool for comparison.

The one-dimensional profiles drawn along [100] and [110] directions are plotted (Fig. 8) for both the data sets measured at

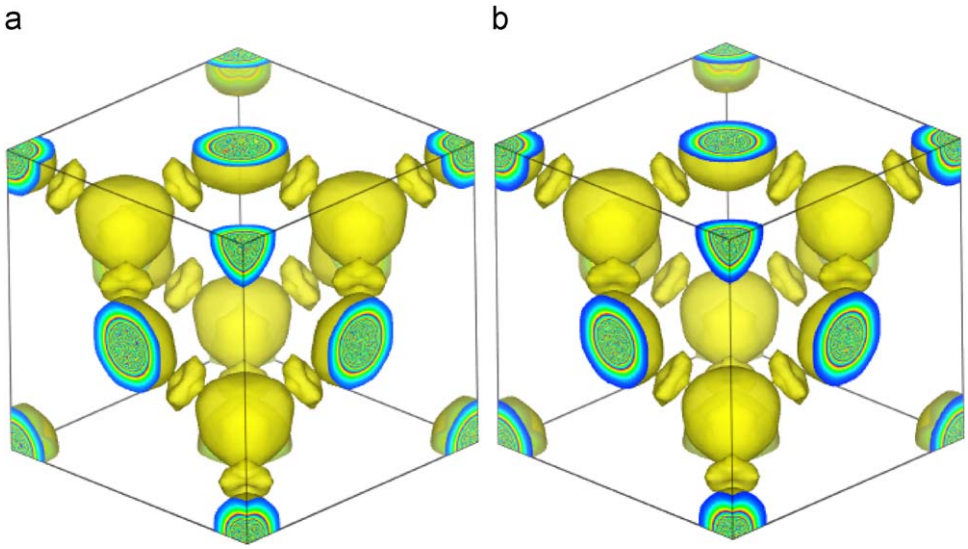

Fig. 4. Three-dimensional charge density in the unit cell of Ge (a) for RT at isosurface level 0.42 e/Å^3 and (b) for 200 K at isosurface level 0.36 e/Å^3.

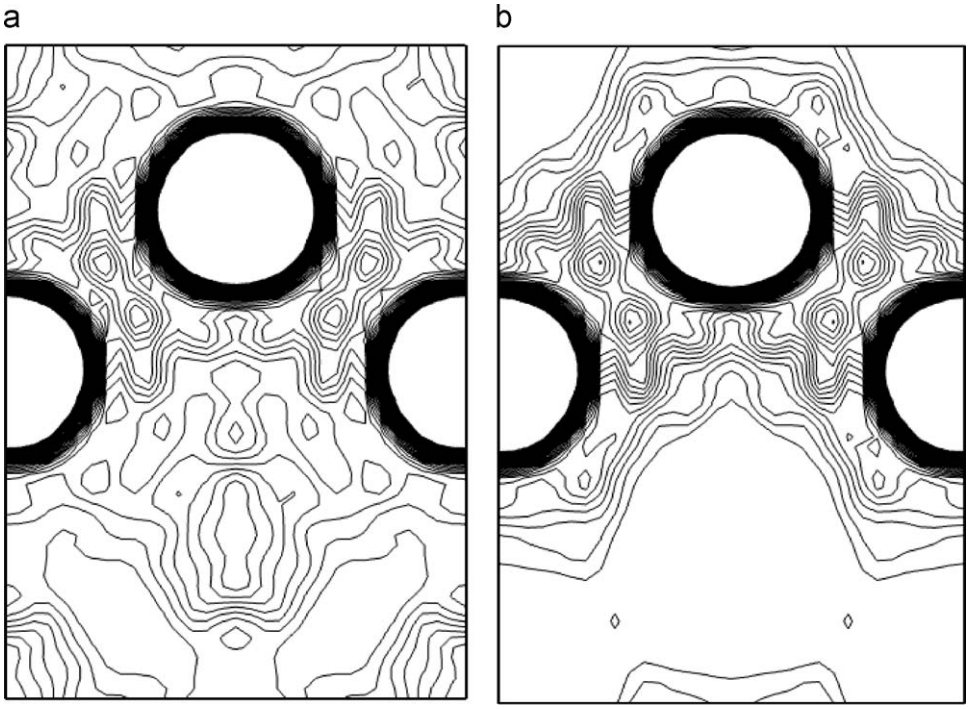

Fig. 5. MEM map on (0 $\bar{1}$ 0) plane for (a) RT, (b) 200 K. Contour ranges from 0.35 to 3.0 e/Å^3. Contour interval is 0.1325 e/Å^3.

RT and 200 K. These profiles show the core of the atom at the corner ends almost near 0.91 Å and is the same that was observed in the bonding direction. The humps and the non-zero densities from there is because of the free spread of the charge densities in the respective directions but the densities assume minimum values at the mid way between the pair of atoms in that direction. It should also be noted that the profiles along [1 0 0], [1 1 0] and [1 1 1] measured at 200 K contract towards the core and this results in the increase in the peak value (at the origin) of the profile measured at the lower temperature than its counter part. This is visualized in Fig. 9. Some important positions and their density values are tabulated in Table 5. These results have credited the MEM method for its accuracy and efficiency in handling the structure factors for the calculation of charge density in the unit cell. The precise charge density especially in the valence region is further analysed for the chemical information using parameters like ρ, $\vec{\nabla}\rho$ and $\nabla^2\rho$. The parameter used for the identification of the shell structure is the Laplacian function.

6. The Laplacian and valence shell charge concentration

The development of "Atoms in molecule" theory [14] aims at the rigorous interpretations of solutions to the Schrödinger

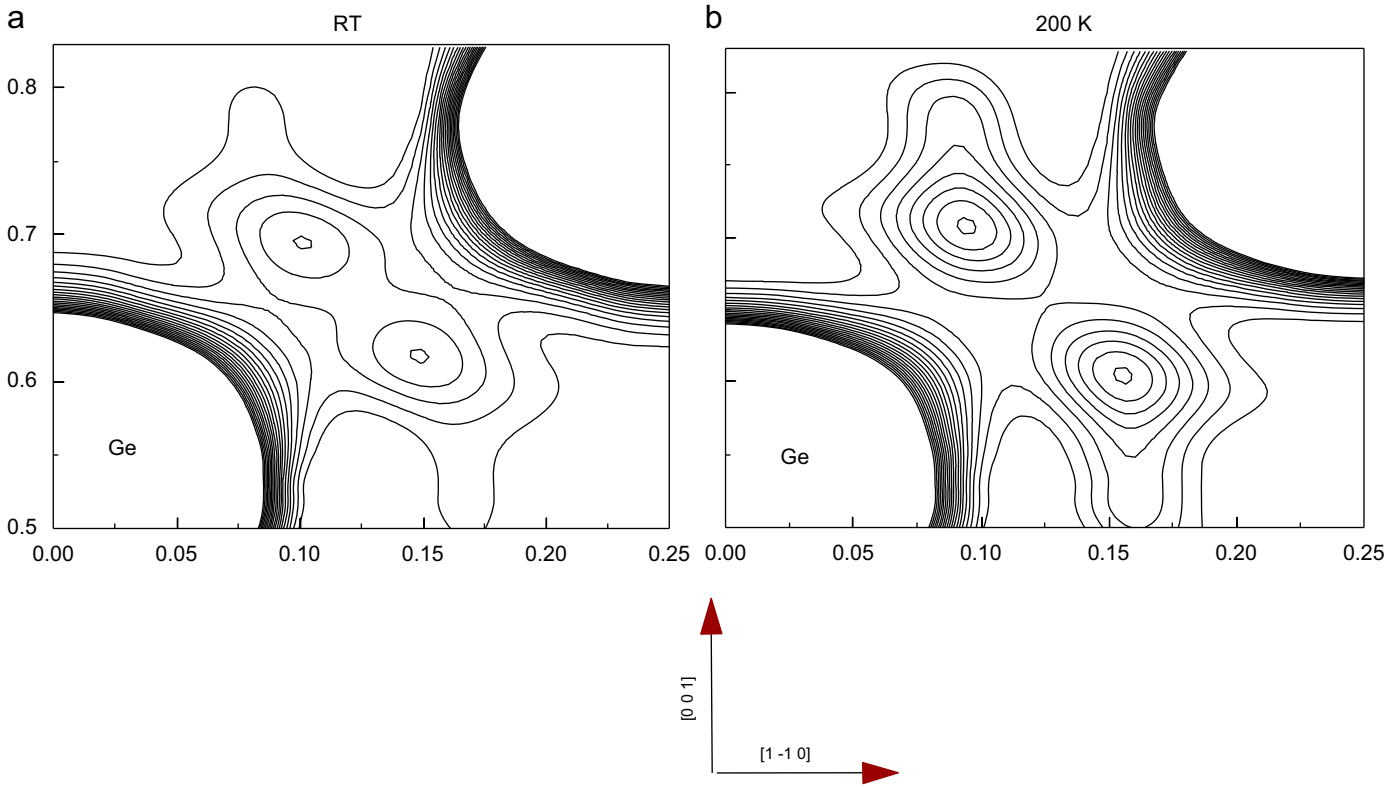

Fig. 6. MEM map on (1–10) plane for (a) RT, (b) 200 K. Contour ranges from 0.35 to 2.05 e/Å^3. Contour interval is 0.085 e/Å^3.

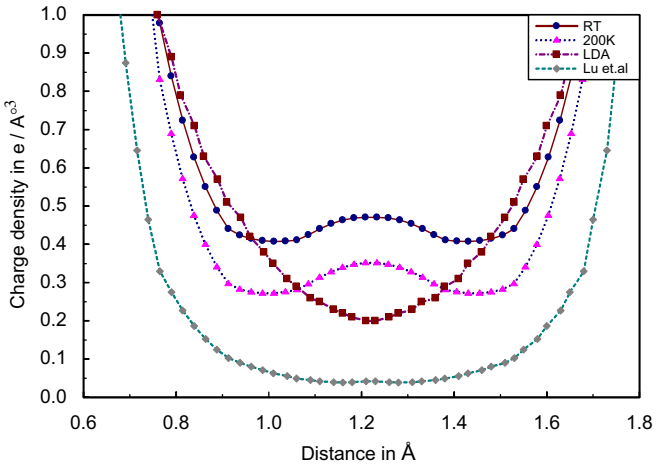

Fig. 7. One-dimensional profiles of electron density along [111] directions.

Table 5
Electron densities and positions from one-dimensional MEM profiles.

Particulars	RT		200 K	
	Position (Å)	Density (e/Å^3)	Position (Å)	Density (e/Å^3)
Along 100 direction				
I minimum	1.322	0.115	1.410	0.155
II minimum	2.821	7.6e−07	2.820	0.030
Along 110 direction				
I minimum	0.997	0.152	0.997	0.247
II minimum	1.995	0.122	1.994	0.155
Along 111 direction				
I minimum	1.069	0.516	1.068	0.474
NNM	1.221	0.555	1.221	0.525
II minimum	1.374	0.516	1.374	0.473
I peak	0.0	775.00	0.0	805.45

equation in terms of chemical concepts. This was achieved partly by the scalar functions $\rho(\mathbf{r})$ and then the Laplacian of the electron density $L(r) = \nabla^2\rho(\mathbf{r})$, which contains wealth of chemical information.

Laplacian supports the valence shell electron pair repulsion model (VSEPR) [24], which redefines acidity in terms of the balance between kinetic and potential energy densities. A direct definition of Laplacian is the sum of eigen values of Hessian of ρ, thus the Laplacian measures the local curvature of a function in all its dimensions. When Laplacian of density is positive, then the density is found to be locally depleted at the point of reference and when it is negative the density is found to be locally concentrated. And thus the magnitude of L(r) determines how strong the effect of electron density concentration or depletion is. This feature can be used for understanding the charge distribution in terms of their spatial distinction of core and valence.

The Laplacian of ρ is not defined at the nucleus because of the presence of cusp and is extremely negative near the nucleus. Moving away from nucleus the $\nabla^2\rho(\mathbf{r})$ goes through zero at a distance r_1 and climbs to a very high positive value and again decreases from the maximum and reaches zero at r_2. The zone from origin to r_2 corresponds to the first principal quantum shell $(n = 1)$ called the K-shell. The zeroes in the Laplacian are the spherical nodes binding the regions of charge depletion or concentration. The next quantum shell called L-shell appears from r_2 to infinity. Since this region constitutes the valence shell we call

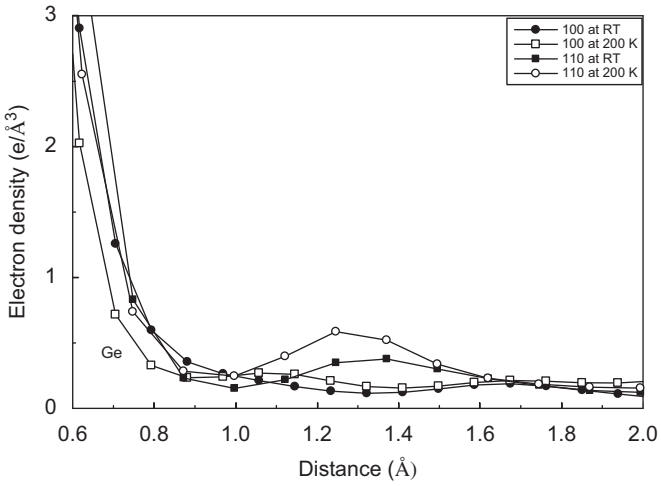

Fig. 8. One-dimensional profiles of electron density along [100] and [110] directions.

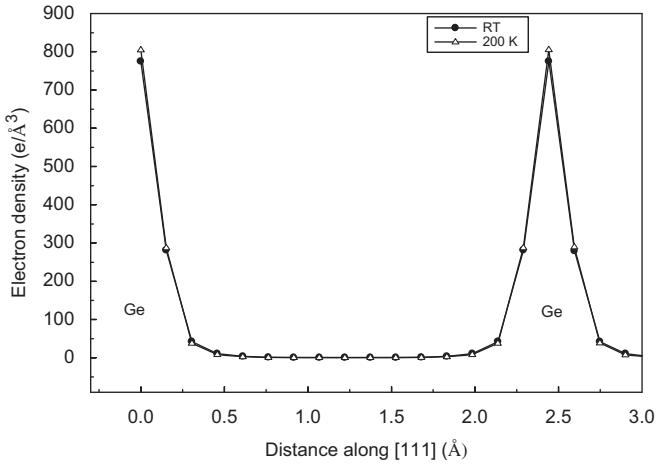

Fig. 9. Variation of Ge peak heights with respect to temperature.

it the region of valence shell charge concentration. Laplacian of the charge density constructed using MEM model is drawn for both the data sets along the bond path and presented as Fig. 10 along with the one calculated from charge density using LDA model. The Laplacian defined near the nucleus produces the first spherical node normally at approximately a radius $1/Z$ (where Z is the atomic number) and this radius is well below our resolution limit i.e. 0.088 Å and hence not observed. The nodes of K-shell and L-shell are identified from the figure and they also seem to shrink as the temperature of the system is lowered. Table 6 illustrates the position of the nodes observed from true positive charge density evaluated using MEM.

To visualize the details of the orbital partitioning and the shell structure through the alternate arrangement of charge concentration and depletion $\nabla^2\rho$ is calculated using the charge density from MEM model and plotted upon the (110) plane for both the data sets (see Fig. 11a and b). These figures show both positive and negative regions (dotted contours) arranged alternatively showing the variations in the region of charge concentration where $\nabla^2\rho<0$ and charge depletion ($\nabla^2\rho>0$). The presence of the valence charge in the non-bonding direction is clearly visualized where $\nabla^2\rho$ is completely negative. The Laplacian function in the bonding region (see inside picture of Fig. 10) is also used to visualize the undulations existing due to the localized orbital arrangement in space. The quantitative analysis of the partitioning of the orbitals and identification of the region of charge concentration/depletion can be done using another function called localized orbital locator proposed by Schmider and Becke [25,26].

Table 6
Positions of the nodes of K-shell (r_1) and L-shell (r_2).

Source function	L(r)		LOL V(r)		ELF	
T (°K)	r_1 (Å)	r_2 (Å)	r_1 (Å)	r_2 (Å)	r_1 (Å)	r_2 (Å)
RT	0.135	0.162	0.1325	0.162	0.1205	0.17
200	0.139	0.159	0.1365	0.155	0.123	0.17
RT_{LDA}	0.125	0.164	0.125	0.1625	0.12	0.17
RT [11]	0.1265	0.167	0.1265	0.165	0.127	0.1625

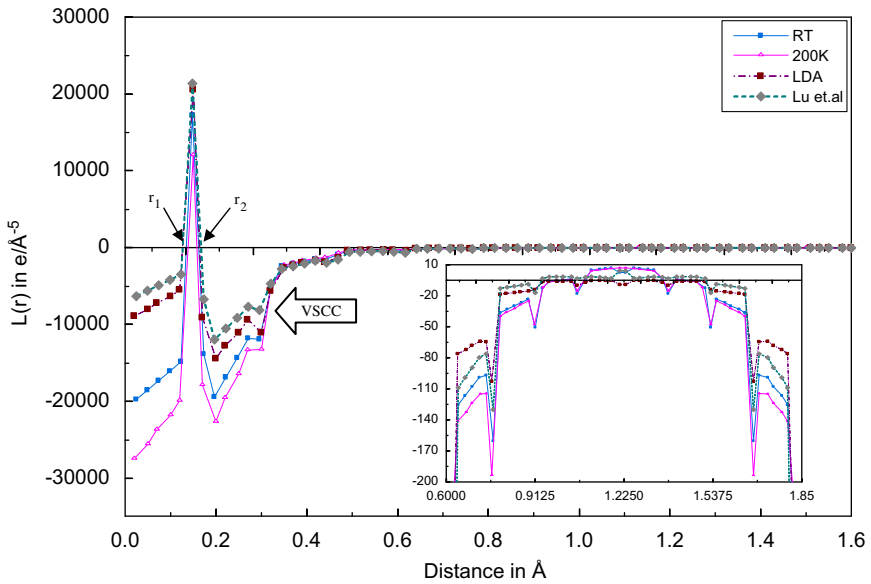

Fig. 10. Profiles of L(r) along the bond path.

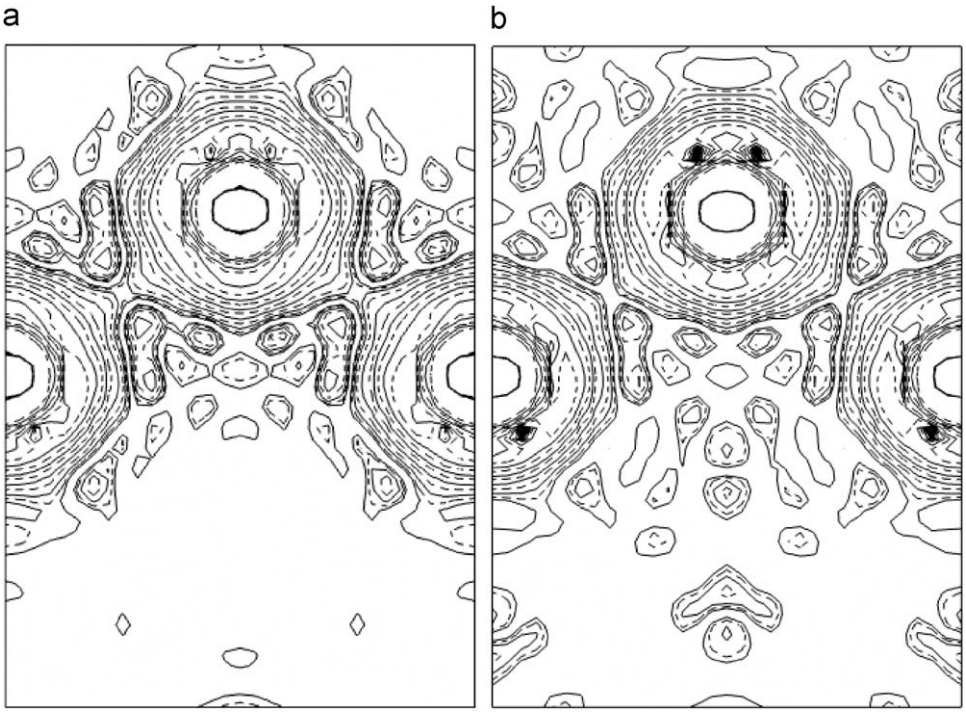

Fig. 11. Map of $\nabla^2\rho(\mathbf{r})$ upon $(1\,\bar{1}\,0)$ plane (a) for RT and (b) for 200 K.

7. Localized orbital locator

The localized orbital locator, which describes the features of bonding in terms of the local kinetic energy, is approximately expressed as a function of electron density and its first and second derivatives. Kinetic energy density becomes small when a single dominating orbital has zero-gradient i.e., a localized orbital has a maximum or saddle point. Otherwise, it becomes large in the space between different localized orbitals. The localization of orbital can be achieved from the measurement of relative velocity of electrons in space.

The measure of relative velocity of electrons at a point **r** in the position space is defined as ([4,25,26])

$$V(\mathbf{r}) = \frac{t(\mathbf{r})}{1 + t(\mathbf{r})}$$

where

$$t(\mathbf{r}) = \frac{D_0(\mathbf{r})}{D_{DFT}(\mathbf{r})}, D_0(\mathbf{r}) = \left(\frac{3}{10}\right)(3\pi^2)^{2/3}[\rho(\mathbf{r})]^{5/3},$$

and

$$D_{DFT} = \left(\frac{3}{10}\right)(3\pi^2)^{2/3}[\rho(\mathbf{r})]^{5/3} - \frac{1}{9}\frac{|\vec{\nabla}\rho(\mathbf{r})|^2}{\rho(\mathbf{r})} + \frac{1}{6}\nabla^2\rho(\mathbf{r})$$

When mapping V in a range of r it gives values of $0 \le V \le 1$. Values of $V > 0.5$ mark the regions where electron's velocity is slower than that in a homogenous electron model ($V = 0.5$). These regions are associated with the localized orbitals describing the electron localization in the covalent bonds and lone pairs. Values of $V < 0.5$ indicate the regions where electron kinetic energy is higher than that in a homogeneous electron gas as it takes place in the ionic and van der Walls bonds with low density.

Approximate magnitudes of localized-orbital locator exhibit all the features displaying the electron concentration and depletion in the position space. Covalent bond shows up a closed region of the LOL values more then 0.5 in inter-nuclear space, while ionic and van der Waals atomic interactions exhibit closed regions of large LOL around nuclear positions and a saddle point (minimum) between them on the inter-atomic line. Electron lone-pairs manifest themselves as local LOL maxima. It is significant that the localized-orbital locator distinguishes not only the covalent, ionic and van der Waals bond but the polar covalent and ionic bonds as well. In this respect, it is superior to the analysis based on Laplacian of the electron density, which does not possess such ability.

LOL is plotted for the Ge atom along its bond path both at RT and 200 K (see Fig. 12), which has shown clearly the positioning of the K- and L-shell (see inside picture of Fig. 12). The positions of r_1 and r_2 discussed in the Laplacian also show up here for LOL and the values are listed in Table 6. The high and low saddles of intermediate regions of charge concentration/depletion can also be identified from LOL function. The rise in LOL above 0.5 in the bonding region ($r > 1.1$ Å) seen from the Fig. 12 reaffirms that the bonding indeed is covalent. The same phenomenon observed in the two-dimensional $\nabla^2\rho$ map upon (110) plane is confirmed here from the LOL function.

8. Electron localization function

Another way of locating the localized pair of electrons is by electron localization function. ELF was introduced by Becke and Edgecombe [27] as a "simple measure of electron localization in atomic and molecular systems". The original formula is based on the Taylor expansion of the spherically averaged conditional same-spin pair probability density to find an electron close to a same-spin reference electron. The main aspect of this formulation is that this defined ELF is a property of the same-spin pair density.

Becke and Edgecombe associated the localization of an electron with the probability density to find a second like-spin electron near the reference point. The smaller this probability

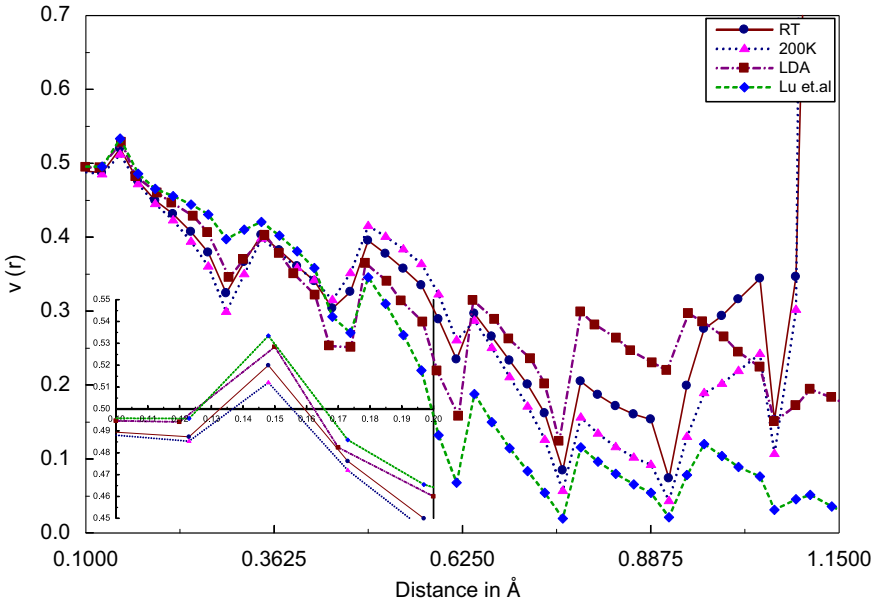

Fig. 12. Profiles of $v(\mathbf{r})$ along the bond path.

density, i.e., the smaller the expression

$$D(\mathbf{r}) = \sum i^{\sigma} |\nabla \psi_i(\mathbf{r})|^2 - \frac{1}{4} |\nabla \rho(\mathbf{r})|^2 / \rho(\mathbf{r})$$

of the quadratic term, the higher localized an electron is. Thus, the Pauli repulsion between two like-spin electrons, described by the smallness of $D(\mathbf{r})$, is taken as a measure of the electron localization. Using the corresponding factor found for uniform homogeneous electron gas $D_h(\mathbf{r})$, Becke and Edgecombe defined ELF as follows:

$$\eta(\mathbf{r}) = 1/[1 + \chi_{\mathrm{BE}}^2(\mathbf{r})]$$

with

$$\chi_{\mathrm{BE}}(\mathbf{r}) = D(\mathbf{r})/D_h(\mathbf{r})$$

where

$$D_h(\mathbf{r}) = 3/5(6\pi^2)^{2/3} \rho(\mathbf{r})^{5/3}$$

Given by the definition, ELF values are bound between 0 and 1. ELF cannot yield the value of $D(\mathbf{r})$ – i.e., the actual measure of the electron localization – because it depends, through $D_h(\mathbf{r})$, on the electron density as well. In this sense, ELF is a relative measure of the electron localization. High ELF values show that at the examined position the electrons are more localized than in a uniform electron gas of the same density. $\eta(\mathbf{r}) = 1/2$ indicates that the effect of the Pauli repulsion is the same as in the uniform electron gas of the same density. The ELF plotted for both the data sets of Ge (Fig. 13) show the positions of the like-spin electron pair and this can be coinciding with the peaks found in LOL.

The ELF is known to be small in the boundary regions of localized orbitals. The maximal values of ELF close to 1 show the existence of pure s orbital and where s and p orbitals coexist yield values closer to 0.8, while those where s, p and d orbitals are present yield values closer to 0.6 [5]. The positions of these orbitals and the boundaries of the localized orbitals for Ge at RT and 200 K are identified from the plot and listed in Table 7. The table gives the positions that are mostly for the s orbital and a very unique position of 0.79 Å where the s, p and d orbitals are located for all the data sets. The positions of $\mathbf{r}_1$ and $\mathbf{r}_2$ discussed in the Laplacian also show up here for ELF (see inside picture of Fig. 13) and the values are listed in Table 6.

The correlation between ELF and chemical bonding is known to be a topological and not an energetical one. And hence ELF can be said to represent the organization of chemical bonding in direct space. Although it has been termed "electron localization function" its relation with the physical concept of localized and delocalized electrons seems to be more subtle. The absolute value of η at critical points does not play a general role. Instead, the topology is analysed. The topological analysis of $\eta(\mathbf{r})$ is performed via its associated gradient vector field $\nabla\eta(\mathbf{r})$. This field is characterized by so-called critical points, where $\nabla\eta(\mathbf{r}) = (0, 0, 0)$. They represent local maxima, minima and saddle points of $\eta(\mathbf{r})$. In three-dimensional space there exist four different types of non-degenerate critical points *viz* attractor (3, −3), repellor (3, 3), and saddle points (3, 1) and (3, −1). The presence of the non-nuclear attractor in the bonding region is attributed to the covalent bonding electron pairs in the chosen system. In our case, the ELF profile drawn at RT shows a (3, −3) at the mid bond position, thus confirming the covalent character in the solid. While the magnitude of ELF at the mid bond position is 0.3998, which is well below the expected value of 0.6 representing the covalent bonding electron pairs. The reason being the dispersed charges in the non-bonding direction resulting in the low value of ELF at the mid bond position. The other ELF profiles failed to enact this behavior mainly due to the charge rearrangement in the non-bonding direction that depletes the valence region. LDA approach and the values correspond to Lu et al. [11] also failed in this front due to the inherent difficulties of these models in defining the valence region. One of the cures could be using the MEM method more effectively by dividing the unit cell into larger number of pixels that results in higher resolution charge density pictures. Nevertheless the experimental charge density is more useful in defining the electronic picture using the tools like ELF has been proved.

9. Conclusion

The qualitative and quantitative analysis of the true valence electron density is made possible with the help of MEM method

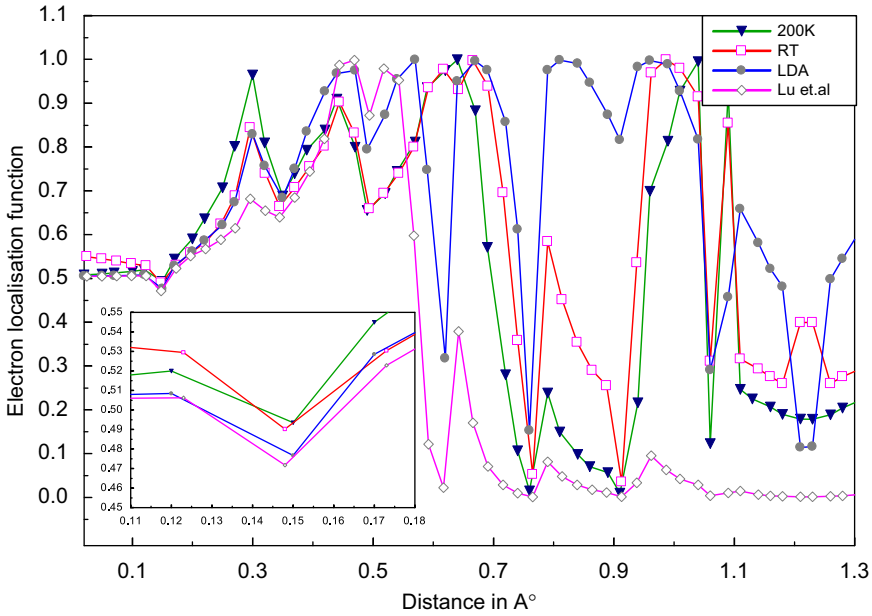

Fig. 13. Profiles of ELF along the bond path.

Table 7
Positions of the nodes of s, p, d orbitals.

Temperature	Function	Position of the nodes in Å						
RT	ELF	0.296	0.444	0.666	0.79	0.987	1.09	–
	LOL	0.345	0.494	0.642	0.79	0.938	1.04	1.18
200 K	ELF	0.3	0.44	0.64	0.79	–	1.04	1.09
	LOL	0.345	0.494	0.642	0.79	0.938	1.04	1.16
RT_{LDA}	ELF	0.3	0.44	0.67	0.81	0.96	–	1.11
	LOL	0.35	0.49	0.64	0.79	0.94	–	–
RT [11]	ELF	0.3	0.48	0.64	0.78	0.96	–	–
	LOL	0.29	0.465	0.63	0.76	0.92	1.06	–

and it gives enormous information on the nature and the measure of bonding charges in the chosen system. MEM gives true density without unrealistic negative contours and thus becoming useful and accurate when the experimental resolution is good. The charge derived properties of the molecules and crystals, which can otherwise be obtained from quantum chemical estimations, are also possible from the density and their derivatives from the charge density distribution reconstructed using this model.

Acknowledgements

One of the authors Dr. S. Israel acknowledges the authorities of the American College, Madurai 625 002, Tamil Nadu, India, for their continuous support and encouragement to complete this research work. The authors are highly indebted for the generous help of Prof. Guru Row of Indian Institute of Science, Bangalore, and for his great motivation and valuable discussions during this work. The authors of the software JANA2006 are gratefully acknowledged for its availability in the internet for free. The authors wish to thank Prof. Sander van Smaalen of University of Bayreuth, Bayreuth, Germany, and Prof. Lukas Palatinus, for some valuable discussions on the working of the software JANA2006. One of the authors (Dr. R. Saravanan) acknowledges the Council of Scientific and Industrial Research (CSIR) for the financial assistance to the research project No.: 03(1138)/09/EMR-II.

References

[1] S. Israel, R. Saravanan, N. Srinivasan, R.K. Rajaram, J. Phys. Chem. Solids 64 (2003) 43.
[2] S. Israel, R. Saravanan, R.K. Rajaram, Physica B349 (2004) 390.
[3] N.K. Hansen, P. Coppens, Acta Crystallogr. A34 (1978) 909.
[4] V. Tsirelson, A. Stash, Acta Crystallogr. B58 (2002) 780–785.
[5] A. Savin, J. Mol. Struct. (Theochem.) (2005) 127–131.
[6] Z.W. Lu, A. Zunger, M. Deusch, Phys. Rev. B 52 (16) (1995–) 11904.
[7] International Tables for X-ray Crystallography, vol. IV, The Kynoch Press, England, 1974.
[8] W.H. Zachariasen, Acta Crystallogr. 23 (1967) 558.
[9] V. Petříček, M Dušek, L. Palatinus, The crystallographic computing system, in: JANA 2006, Institute of Physics, Academy of Sciences of the Czech Republic, Praha, 2006.
[10] E. Clementi, C. Roetti, Roothaan-Hatree-Fock atomic wave functions, At. Data Nucl. Data Tables 14 (1974) 177–478.
[11] Z.W. Lu, A. Zunger, M. Deusch, Phys. Rev. B 47 (1993) 9385.
[12] B. Dawson, Proc. R. Soc. London Ser. A 298 (1967) 255–263;
B. Dawson, Proc. R. Soc. London Ser. A 298 (1967) 264–288.
[13] R.F. Stewart, J. Chem. Phys. 58 (1973) 1668.
[14] R.F.W. Bader, Atoms in Molecules—A Quantum Theory, Oxford University Press, Oxford, 1990.
[15] A. Avilov, G. Lepeshov, U. Pietsch, V. Tsierelson, J. Phys. Chem. Solids 62 (2001) 2135.
[16] V.G. Tsierelson, Acta crystallogr. A55 (1999) supplement, Abstract M 13-OF-003, 1999.
[17] Y.A. Abramov, F.P. Okamura, Acta Crystallogr. A 53 (1997) 187.
[18] D.M. Collins, Nature 298 (1982) 49.
[19] M. Sakata, M. Sato, Acta Crystallogr. A 46 (1990) 263.
[20] K. Momma, F. Izumi, VESTA: a three-dimensional visualization system for electronic and structural analysis, J. Appl. Crystallogr. 41 (2008) 653–658.
[21] C.S. Wang, B.M. Klein, Phys. Rev. B 24 (1981) 3393.
[22] F.H. Allen, O. Kennard, D.G. Watson, L. Brammer, A.G. Orpen, R. Taylor, J. Chem. Soc. Perkin Trans. II 1 (1987) S1.
[23] K. Yamamoto, Y. Takahashi, K. Ohshima, F.P. Okamura, K. Yukino, Acta Crystallogr. A52 (1996) 606.
[24] R.J. Gillespie, R.S.Q. Nyholm, Rev. Chem. Soc. 11 (1957) 339.
[25] H.L. Schmider, A.D. Becke, J. Mol. Struct. (Theochem.) 527 (2000) 51–61.
[26] H.L. Schmider, A.D. Becke, J. Chem. Phys. 116 (2002) 3184–3193.
[27] A.D. Becke, K.E. Edgecombe, J. Chem. Phys. 92 (1990) 5397.